Rapid Communications

Robust skyrmion-bubble textures in $SrRuO_3$ thin films stabilized by magnetic anisotropy

P. Zhang,[1,*] A. Das,[1] E. Barts,[1] M. Azhar,[1] L. Si,[2] K. Held,[2] M. Mostovoy,[1] and T. Banerjee[1,†]
[1]*Zernike Institute for Advanced Materials, University of Groningen, 9747 AG Groningen, The Netherlands*
[2]*Institut für Festkörperphysik, TU Wien, Wiedner Hauptstrae 8-10, 1040 Vienna, Austria*

(Received 10 January 2020; accepted 14 July 2020; published 27 July 2020)

Topological spin textures in the itinerant ferromagnet $SrRuO_3$ are studied combining Hall transport measurements and numerical simulations. We observe characteristic signatures of the topological Hall effect associated with skyrmions. A relatively large thickness of our films and the absence of heavy-metal layers make the interfacial Dzyaloshinskii-Moriya interaction an unlikely source of these topological spin textures. In addition, the transport anomalies exhibit an unprecedented robustness to magnetic field tilting and temperature variations. Our numerical simulations suggest that this unconventional behavior results from compact magnetic bubbles with skyrmion topology stabilized by magnetodipolar interactions and higher-order magnetocrystalline ansiotropies in an unexpected region of parameter space. This work presents a comprehensive understanding of the origin of the topological Hall effect in $SrRuO_3$, incorporating the complex angular dependence of the magnetic anisotropy, intrinsic to this material.

DOI: 10.1103/PhysRevResearch.2.032026

I. INTRODUCTION

The interplay between magnetism and electronic transport, enabled by spin-orbit coupling, has been explored to the study of different phenomena such as the anomalous Hall effect (AHE) [1–4], anisotropic magnetoresistance [5,6], and the extrinsic and intrinsic spin Hall effect [7–9]. Of them, the AHE has been widely pursued for over a century due to its rich physics in diverse magnetic systems. It originates from intrinsic and extrinsic contributions to quantum transport in magnetic materials, i.e., the Berry curvature of the electronic bands and impurity scattering. The contribution of the AHE to electronic transport, namely, in Hall resistivity is represented as $\rho_{\mathrm{AHE}} = R_s M$, relating it to the magnetization (M), while R_s incorporates mechanisms that combine exchange interactions with spin-orbit coupling effects. More recently, the topological Hall effect (THE), an additional component to the Hall resistivity [10–15], resulting from an effective Lorentz force by a topological spin texture, has been reported for systems with negligible and sizable spin-orbit coupling. The scalar chirality of noncoplanar spin structures, such as the magnetic skyrmion, gives rise to an effective magnetic field with a quantized flux proportional to the topological skyrmion number [16,17]. Widely investigated in the context of the THE are the bulk chiral magnets as well as multilayers of conventional magnets with heavy-metal materials [18–22], offering novel physics with prospects of applications in nonvolatile memory devices.

The material class of correlated oxides has garnered recent attention in the exploration of skyrmions [23,24] and exploiting the THE [25], particularly in the itinerant ferromagnet $SrRuO_3$ (SRO) [26–29]. Spin-orbit coupling has been exploited earlier, to the study of different emergent phenomena in SRO [30–35] and more recently to the study of the THE [26–28] in devices utilizing SRO interfaced or capped with $SrIrO_3$ (SIO) and ascribed to skyrmion textures. However, the understanding and origin of such magnetic textures that lead to the observation of THE is surprisingly lacking. For an itinerant ferromagnet such as SRO, it is expected that the competition between different magnetic energies such as magnetocrystalline anisotropy, long-range magnetodipolar forces, and the interfacial Dzyaloshinskii-Moriya interaction (DMI), when appropriately tailored, can give rise to new magnetic textures. Despite this, such an interplay between magnetic energies in electronic transport was not addressed in experimental and in theoretical studies. This is quintessential not only for a comprehensive understanding of the origin of the THE but also for their stabilization and manipulation by applied currents or electric fields.

In this Rapid Communication, we report unconventional features in the Hall transport in SRO films, akin to recent studies on THE in SIO/SRO bilayers [26,36] that were ascribed to skyrmions. Our films are tailored to be ferromagnetic and multidomain, thus expected to display a complex magnetocrystalline anisotropy dependence both with the applied magnetic field and temperature below the magnetic phase transition temperature (T_C) of 120 K. We invoke the role of magnetostatic interactions, anisotropies, and interfacial DMI to model the magnetic textures and explain our experimental findings by the formation of magnetic bubble domains with skyrmion topology. The robustness of the bubble arrays against the rotation of the magnetic field vector, unique to our

*p.zhang@rug.nl
†t.banerjee@rug.nl

findings, as well as the relatively high critical magnetic fields, are studied and related to the complex angular dependence of the magnetic anisotropy energy in our SRO films.

II. EXPERIMENTAL DETAILS

SRO, an archetypal member of the ruthenate family, is an itinerant ferromagnet with large spin-orbit coupling and a complex magnetocrystalline anisotropy dependence [35,37,38] with a temperature below the T_C of 150–160 K in the bulk. Epitaxial SRO films were deposited on terminated and annealed (100) $SrTiO_3$ (STO) single-crystal substrates by pulsed laser deposition (PLD). All the films discussed in this work (A and B in the main text and C in the Supplemental Material) [39] are compressively strained with a lattice mismatch of 0.64% with STO and 8.7 ± 0.2 nm thick. Further information on the films is summarized in the Supplemental Material [39] (Figs. S1 and S2 and Table I). The atomic force microscopy (AFM) topology (Fig. S2) before and after the thin-film deposition reveals the presence of both TiO_2 and SrO surface termination. Such double-terminated substrates were found to result in local differences in structural and electronic properties at the different terminating sites, [34] and are an important consideration here.

III. MAGNETIZATION AND ELECTRONIC TRANSPORT STUDIES

Magnetization studies of film B along the in-plane and out-of-plane directions are shown in Fig. 1(a) and is suggestive of multiaxial magnetocrystalline anisotropy [31,35]. The easy axis of such strained thin films has a strong temperature-dependent angular variation with the film normal, leading to a complex magnetocrystalline anisotropy, as reported in earlier studies [35,40].

Subsequently the films were patterned into a Hall bar geometry [Fig. 2(a)] using standard lithography techniques and ion beam etching for Hall transport studies. The transverse resistivity ρ_{xy} can be written as the sum of the following contributions, $\rho_{xy} = R_o B_\perp + R_s M_\perp(B_\perp) + \rho_{\mathrm{THE}}$, and is antisymmetric in both **B** and **M**. The first term is due to the ordinary Hall effect (OHE), and the second and third terms are due to AHE and the THE, respectively. Figure 1(b) shows the scaling of the anomalous Hall resistivity ρ_{AHE} for films A and B with temperature. ρ_{AHE} is obtained from the zero-field resistivity after the subtraction of the ordinary Hall background (details in Supplemental Material [39] and in Fig. S4). ρ_{AHE} for all the films in this work have been obtained with an out-of plane magnetic field and at different temperatures as shown in Figs. 1(d) and 2(b). A nonmonotonous dependence of ρ_{AHE} is found for both samples with temperature. Film A exhibits a sign reversal with temperature, whereas film B shows no such reversal. Such trends, typical of SRO films, indicate the intrinsic origin of the AHE associated with the intricacies of the temperature modulations in the band structure and their crossings at the Fermi energy [10,14,30,31]. The differences in the trend, on the other hand, between the two films, are a manifestation of the local changes in the crystalline lattice structure and their corresponding influence on the band structure.

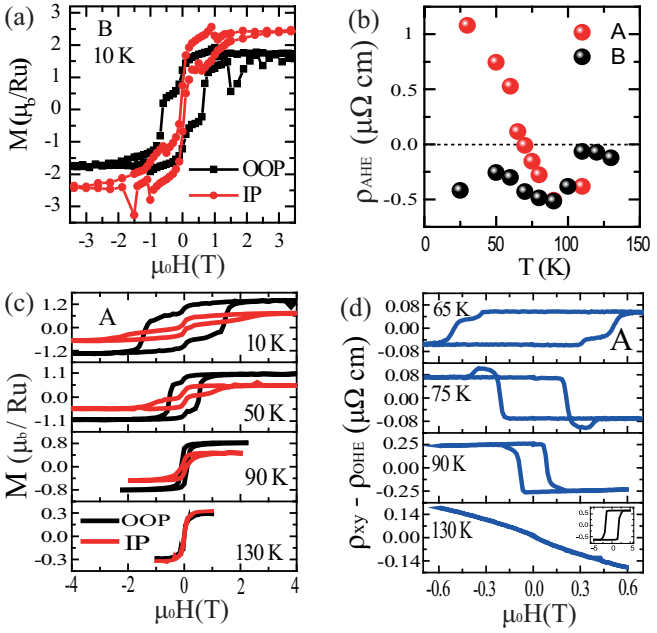

FIG. 1. (a) *M-H* curves measured at 10 K for film B in out-of-plane (black) and in-plane (red) directions, respectively. (b) Temperature dependence of anomalous Hall resistivity (ρ_{AHE}) for films A and B. Film A shows a sign change in ρ_{AHE} unlike film B. (c) *M-H* for out of plane (black) and in plane (red) at different temperatures for film A. Between each measurement, the film was warmed to 300 K and thereafter cooled to the measurement temperature. (d) Magnetic-field-dependent Hall resistivity measured at different temperatures for film A. The inset shows the Hall resistivity at 10 K which changes sign beyond 70 K.

A comprehensive study of the temperature dependence of the magnetization was carried out for both in-plane and out-of-plane configurations and shown in Fig. 1(c) is for film A. The temperature dependence of the magnetization shows the evolution of a complex magnetocrystalline anisotropy in SRO, as discussed in Refs. [35,40] and consistent with the occurrence of an easy-plane anisotropy. Figures 1(d) and 2(b) show the magnetic field dependence of the electronic transport in films A and B, respectively, patterned into a Hall bar with a channel width of 50 μm. The direction of the applied field is shown in Fig. 2(a). Distinct features can be seen—the atypical AHE contribution corresponding to the magnetization of the films and its temperature dependence and the enhancement in transverse resistivity ρ_{xy} at higher fields manifested as humps in the ρ_{xy} loops. The AHE signal is generally assumed to be proportional to the magnetization, obtained from the *M-H* loops, enabling the extraction of the THE contribution, although a direct correlation of the coercive fields H_c obtained from bulk magnetization studies and from AHE are nontrivial.

We further observe additional humps in ρ_{xy} up to the T_C for the films studied [Figs. 1(d) and 2(b)–2(d)] and that are commonly ascribed to the THE, originating from the skew scattering off an effective magnetic field induced by noncoplanar topological spin textures. The humps appear irrespective of the differences in either the sign of the AHE or in the magnetocrystalline anisotropy in films A and B. The THE

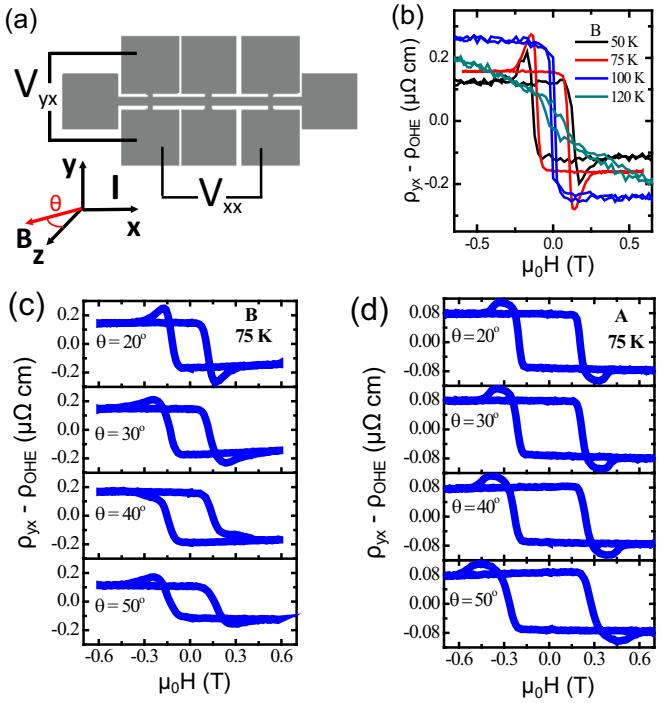

FIG. 2. Field- and angle-dependent Hall resistivity of SRO thin films. (a) Hall bar schematic showing longitudinal (V_{xx}) and transverse contact voltage contacts (V_{yx}). The tilt angle θ with the magnetic field B in the out-of-plane direction and the current (I) along the x direction are also shown. (b) Field-dependent Hall resistivity at different temperatures for film B. The linear contribution from OHE has been subtracted (except for 120 K). (c), (d) Angular-dependent Hall resistivity at 75 K for films B and A, respectively.

in all cases is observed above 30 K and persists up to the T_C of the films, while being remarkably robust to a large tilting angle with the applied field as shown in Figs. 2(c) and 2(d). These unique findings, reported in nonchiral and relatively thick SRO films, imprint signatures of the complex temperature dependence of the multiple uniaxial anisotropies intrinsic to SRO and are associated with skyrmion bubbles. Upon increasing the magnetic field above 0.25 T, the THE was found to vanish in both films, corresponding to the collapse of topological spin textures as the magnetization reaches saturation, as shown in Figs. 1(d) and 2(b).

IV. NUMERICAL SIMULATIONS

To understand the occurrence of THE and the stability of the magnetic bubble array in our films, we performed numerical simulations, with the simplifying assumption that the magnetization vector in thin SRO film is independent of the vertical coordinate z: $\boldsymbol{M} = \boldsymbol{M}(x, y)$ [41]. The energy of the film of thickness h is

$$E = h \int d^2x \left[\sum_{i=x,y} \frac{c}{2} (\partial_i \boldsymbol{M})^2 - \frac{K_1}{2} M_z^2 - \frac{K_2}{4M_s^2} M_z^4 - \boldsymbol{H} \cdot \boldsymbol{M} + \frac{\lambda}{4M_s^2} \left(\boldsymbol{M}^2 - M_s^2 \right)^2 \right] + E_{\rm ms}, \quad (1)$$

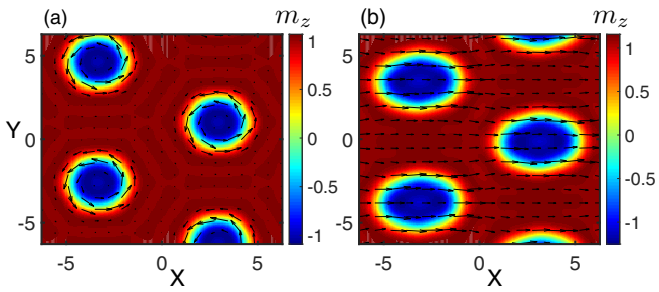

FIG. 3. Arrays of bubbles (a) with topological charge -1 and (b) carrying zero topological charge and an in-plane magnetic moment. In-plane components of $\boldsymbol{m}$ are shown with arrows, and m_z is color coded. Distances are given in units of the film thickness h.

where the first term is the exchange energy, the second and third terms are the magnetocrystalline anisotropy energies of second and fourth order, respectively, and the fourth term is the Zeeman energy (in cgs units). Rather than considering Landau expansion in powers of M [41], we use the fifth term in Eq. (1) with the parameter $\lambda = 100$ to constrain the magnitude of the magnetization to its saturation value, $\boldsymbol{M} = M_s \boldsymbol{m}$ ($\boldsymbol{m}^2 = 1$). The energy of magnetostatic interactions $E_{\rm ms}$ has a compact form in the reciprocal space [42]. We minimize energy on the space of 61 Fourier harmonics of the magnetization, which is sufficient to describe the triangular array of Bloch skyrmions (type-I bubbles) with the topological charge -1 [Fig. 3(a)] stabilized by magnetostatic interactions and a magnetic field normal to the film, an array of type-II bubbles with zero topological charge favored by tilted magnetic fields [Fig. 3(b)], and the stripe domain state appearing in weak applied fields (see Ref. [39] for details).

Earlier studies of relatively thick films suggested that stability of the stripe domain state and bubble array requires the quality factor $Q = \frac{K_1}{4\pi} > 1$ [43–45]. For $Q < 1$, the perpendicular magnetic anisotropy is not strong enough to overcome magnetostatic interactions favoring a uniform state with an in-plane magnetization. However, recent studies on Fe/Gd multilayers and micromagnetic simulations of thin films showed that inhomogeneous magnetic states can be induced by an applied magnetic field even for $Q < 1$ [46,47]. This is partly related to the fact that in thin films the domain wall width is no longer negligibly small compared to the film thickness, as can be seen from Fig. 3. In addition, the notion of an effective magnetic anisotropy, $K_{\rm eff} = K_1 - 4\pi$, is only meaningful for uniform states, since dipole-dipole interactions strongly depend on the magnetic modulation wave vector.

Moreover, the phase diagram in Figs. 4(a) and 4(b), calculated for the magnetic field normal to the film, shows that the field interval in which the skyrmion crystal (SkX) has the lowest energy widens as the quality factor decreases. The SkX becomes unstable for $Q \lesssim 0.75$, near the line separating the uniform states with the perpendicular (white color) and tilted (red color) magnetization. The stability region of the SkX phase extends to lower Q and higher critical fields when we include the fourth-order magnetocrystalline anisotropy, which is relatively large in SRO due the strong spin-orbit coupling of Ru [37,38]. Figure 4(b) shows the phase diagram calculated

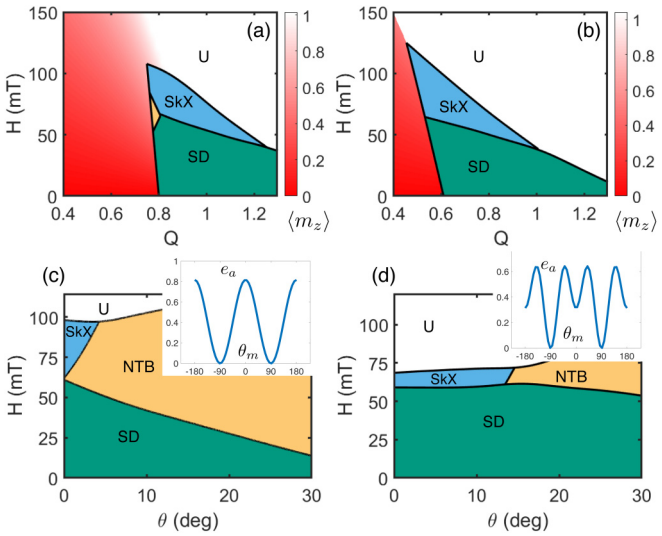

FIG. 4. Magnetic field H vs quality factor $Q = \frac{K_1}{4\pi}$, phase diagrams, which include the skyrmion crystal (SkX), stripe domain (SD), an array of nontopological bubbles (NTBs, yellow), and uniform (U) states. Red color intensity indicates m_z in the uniform state with a tilted magnetization. The state with the magnetization normal to the film is shown with white color. These diagrams are calculated for (a) $R = \frac{K_2}{4\pi} = 0$ and (b) $R = 0.4$. Phase diagrams in a tilted magnetic field, θ being the tilt angle, for (c) $Q = 0.87$ and $R = 0$ and (d) $Q = 0.65$ and $R = 0.60$. The insets show the dependence of the dimensionless anisotropy energy density e_a in the uniform state on the magnetization tilt angle θ_m for the corresponding parameter sets.

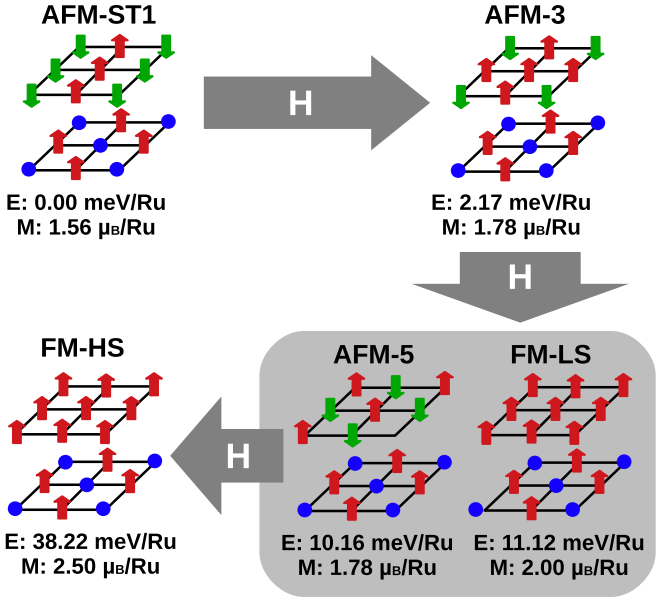

FIG. 5. Schematic picture of ferromagnetic (FM) and antiferromagnetic (AFM) phases and transitions in an external magnetic field as calculated by DFT + U (further details in Ref. [39]). The ↑ and ↓ spins are on the Ru sites, and the (blue) circles are nonmagnetic Ti sites (shown are only the Ru-Ti intermixed and the neighboring Ru layer). E is the zero-field energy of the phase and the M magnetic moment per Ru atom. The gray box indicates the possible coexistence of the AFM-5 and FM-low-spin (LS) phase.

for $R = \frac{K_2}{4\pi} = 0.4$. $R > 0$ favors magnetization normal to the film, which makes the SkX more stable. Thus a smaller quality factor in combination with a higher-order anisotropy can significantly increase the stability of the SkX, although the fields at which the SkX undergoes a transition into a uniform state are still two to three times lower than the field of ∼400 mT at which the THE disappears in experiment. The magnetization relaxation along the z direction and finite-size effects [47] can further increase the stability of topological skyrmions.

In tilted magnetic fields [see Figs. 4(c) and 4(d)] the bubbles with skyrmion topology become unstable and transform into nontopological bubbles (NTBs) with two Bloch points and an in-plane magnetic dipole moment [Fig. 3(b)], resulting in the disappearance of the THE. In the M-type hexaferrite with $Q \sim 1$, the topological phase disappears at a small tilt angle, $\theta = 2.3°$ [42]. The THE found at much larger θ in our experiment can be explained by strong fourth-order anisotropy [see Figs. 4(c) and 4(d)]. The insets show an angular dependence of the anisotropy energy in the uniform state as a function of the magnetization tilt angle θ_m. As R increases, the anisotropy energy, in addition to the global minimum at $\theta_m = \pm\frac{\pi}{2}$ (in-plane magnetization), acquires a local minimum at $\theta_m = 0, \pi$ (out-of-plane magnetization), which leads to an increase of the field tilt angle θ, at which the THE disappears.

The interfacial Dzyaloshinskii-Moriya interaction is effectively small due to the large number of magnetic RuO_2 layers in the SRO film and the absence of heavy-metal elements. However, it can make skyrmions more resilient to the strength and tilt of the applied magnetic field (see Figs. S8 and S9).

V. DENSITY FUNCTIONAL THEORY CALCULATIONS

Finally, we address the differences in the magnetic properties of the films deposited under similar conditions [Figs. 1(a) and 1(c)]. Films A and B display two consecutive transitions below 70 K representative of a metamagnetic behavior. Using density functional theory (DFT)+U, we can explain the differences between them by considering the differences in the Ti intermixing at the SRO/STO interface. We find that Ti intermixing stabilizes different magnetic phases with similar energies (see Fig. 5 and Supplemental Material [39]), including a FM high-spin (HS) state with a magnetic moment of $2.5\mu_B$/Ru as observed for film B [Fig. 1(a)]. The DFT + U calculated magnetic moments and transitions agree well with our key experimental observations.

VI. CONCLUSIONS

The observation of the THE in thick nonchiral SRO films, in the absence of heavy-metal layers, is ascribed to robust magnetic bubble domains with skyrmion topology and explained by incorporating the hitherto ignored contributions of the second- and fourth-order magnetocrystalline anisotropy terms to the total energy and for $Q < 1$. We find that the robustness of such bubble domains against the rotation of the magnetic field vector is significantly influenced by the

complex angular dependence of the multiaxial anisotropy energy in SRO films. These considerations were surprisingly lacking in recent studies [26–28,36] carried out in relatively thinner SRO films using AHE and magnetic force microscope techniques. We believe that the strong temperature dependence of the multiaxial anisotropy makes it challenging to study skyrmions in these thick films using magnetic force microscopy measurements with reasonable spatial and temporal resolution. Such a nontrivial competition between different local and nonlocal magnetic energies by designing magnetocrystalline anisotropies at engineered interfaces opens new opportunities for their manipulation by electric fields and spin-orbit fields for diverse applications in spintronics.

ACKNOWLEDGMENTS

P.Z. thanks China Scholarship Council, and M.A. and A.D. acknowledge Dieptestrategie grants, Zernike Institute for Advanced Materials, for financial support. P.Z., A.D., and T.B. acknowledge J. Baas, J. G. Holstein, and H. H. de Vries for technical assistance and A. A. Burema, S. Chen, and J. J. L. van Rijn for discussions. We thank Christos Panagopoulos for insightful discussions and useful comments. T.B. acknowledges discussions with M. A. Frantiu on micromagnetic simulations. This work was realized using NanoLab-NL facilities. L.S. and K.H. have been supported by the Austrian Science Fund (FWF) through Project No. P30997. E.B. and M.M. acknowledge Vrije FOM-programma "Skyrmionics."

[1] R. Karplus and J. M. Luttinger, Hall effect in ferromagnetics, Phys. Rev. **95**, 1154 (1954).
[2] J. Smit, The spontaneous Hall effect in ferromagnetics I, Physica **21**, 877 (1955).
[3] L. Berger, Side-jump mechanism for the Hall effect of ferromagnets, Phys. Rev. B **2**, 4559 (1970).
[4] N. Nagaosa, J. Sinova, S. Onoda, A. H. MacDonald, and N. P. Ong, Anomalous Hall effect, Rev. Mod. Phys. **82**, 1539 (2010).
[5] I. A. Campbell, A. Fert, and O. Jaoul, The spontaneous resistivity anisotropy in Ni-based alloys, J. Phys. C: Solid State Phys. **3**, S95 (1970).
[6] J. Smit, Magnetoresistance of ferromagnetic metals and alloys at low temperatures, Physica **17**, 612 (1951).
[7] J. E. Hirsch, Spin Hall Effect, Phys. Rev. Lett. **83**, 1834 (1999).
[8] M. I. D'yakonov and V. I. Perel, Possibility of orienting electron spins with current, JETP Lett. **13**, 657 (1971).
[9] J. Sinova, D. Culcer, Q. Niu, N. A. Sinitsyn, T. Jungwirth, and A. H. MacDonald, Universal Intrinsic Spin Hall Effect, Phys. Rev. Lett. **92**, 126603 (2004).
[10] J. Ye, Y. B. Kim, A. J. Millis, B. I. Shraiman, P. Majumdar, and Z. Tešanović, Berry Phase Theory of the Anomalous Hall Effect: Application to Colossal Magnetoresistance Manganites, Phys. Rev. Lett. **83**, 3737 (1999).
[11] M. V. Berry, Quantal phase factors accompanying adiabatic changes, Proc. R. Soc. London, Ser. A **392**, 45 (1984).
[12] A. N. Bogdanov and U. K. Rößler, Chiral Symmetry Breaking in Magnetic Thin Films and Multilayers, Phys. Rev. Lett. **87**, 037203 (2001).
[13] A. Soumyanarayanan, N. Reyren, A. Fert, and C. Panagopoulos, Emergent phenomena induced by spin-orbit coupling at surfaces and interfaces, Nature (London) **539**, 509 (2016).
[14] P. Bruno, V. K. Dugaev, and M. Taillefumier, Topological Hall Effect and Berry Phase in Magnetic Nanostructures, Phys. Rev. Lett. **93**, 096806 (2004).
[15] P. Bruno, Geometrically Constrained Magnetic Wall, Phys. Rev. Lett. **83**, 2425 (1999).
[16] N. Nagaosa and Y. Tokura, Topological properties and dynamics of magnetic skyrmions, Nat. Nanotechnol. **8**, 899 (2013).
[17] Y. Taguchi, T. Sasaki, S. Awaji, Y. Iwasa, T. Tayama, T. Sakakibara, S. Iguchi, T. Ito, and Y. Tokura, Magnetic Field Induced Sign Reversal of the Anomalous Hall Effect in a Pyrochlore Ferromagnet $Nd_2Mo_2O_7$: Evidence for a Spin Chirality Mechanism, Phys. Rev. Lett. **90**, 257202 (2003).
[18] A. Neubauer, C. Pfleiderer, B. Binz, A. Rosch, R. Ritz, P. G. Niklowitz, and P. Böni, Topological Hall Effect in the *A* phase of MnSi, Phys. Rev. Lett. **102**, 186602 (2009).
[19] S. Mühlbauer, B. Binz, F. Jonietz, C. Pfleiderer, A. Rosch, A. Neubauer, R. Georgii, and P. Böni, Skyrmion lattice in a chiral magnet, Science **323**, 915 (2009).
[20] C. Pappas, E. Lelievre-Berna, P. Falus, P. M. Bentley, E. Moskvin, S. Grigoriev, P. Fouquet, and B. Farago, Chiral Paramagnetic Skyrmion-like Phase in MnSi, Phys. Rev. Lett. **102**, 197202 (2009).
[21] M. Lee, W. Kang, Y. Onose, Y. Tokura, and N. P. Ong, Unusual Hall Effect Anomaly in MnSi under Pressure, Phys. Rev. Lett. **102**, 186601 (2009).
[22] A. Soumyanarayanan, M. Raju, A. L. G. Oyarce, A. K. C. Tan, M.-Y. Im, A. P. Petrović, P. Ho, K. H. Khoo, M. Tran, C. K. Gan *et al.*, Tunable room-temperature magnetic skyrmions in Ir/Fe/Co/Pt multilayers, Nat. Mater. **16**, 898 (2017).
[23] J. Rowland, S. Banerjee, and M. Randeria, Skyrmions in chiral magnets with Rashba and Dresselhaus spin-orbit coupling, Phys. Rev. B **93**, 020404(R) (2016).
[24] S. Banerjee, J. Rowland, O. Erten, and M. Randeria, Enhanced Stability of Skyrmions in Two-Dimensional Chiral Magnets with Rashba Spin-Orbit Coupling, Phys. Rev. X **4**, 031045 (2014).
[25] L. Vistoli, W. Wang, A. Sander, Q. Zhu, B. Casals, R. Cichelero, A. Barthélémy, S. Fusil, G. Herranz, S. Valencia *et al.*, Giant topological Hall effect in correlated oxide thin films, Nat. Phys. **15**, 67 (2019).
[26] J. Matsuno, N. Ogawa, K. Yasuda, F. Kagawa, W. Koshibae, N. Nagaosa, Y. Tokura, and M. Kawasaki, Interface-driven topological Hall effect in $SrRuO_3$-$SrIrO_3$ bilayer, Sci. Adv. **2**, e1600304 (2016).
[27] K.-Y. Meng, A. S. Ahmed, M. Baẗani, A.-O. Mandru, X. Zhao, N. Bagueẗs, B. D. Esser, J. Flores, D. W. McComb, H. J. Hug *et al.*, Observation of nanoscale skyrmions in $SrIrO_3$/$SrRuO_3$ bilayers, Nano Lett. **19**, 3169 (2019).
[28] D. J. Groenendijk, C. Autieri, T. C. van Thiel, W. Brzezicki, J. R. Hortensius, D. Afanasiev, N. Gauquelin, P. Barone, K. H. W. van den Bos, S. van Aert, J. Verbeeck, A. Filippetti, S. Picozzi,

M. Cuoco, and A. D. Caviglia, Berry phase engineering at oxide interfaces, Phys. Rev. Research **2**, 023404 (2020).

[29] B. Sohn, B. Kim, S. Y. Park, H. Y. Choi, J. Y. Moon, T. Choi, Y. J. Choi, T. W. Noh, H. Zhou, S. H. Chang *et al.*, Emergence of robust 2D skyrmions in $SrRuO_3$ ultrathin film without the capping layer, arXiv:1810.01615.

[30] Y. Kats, I. Genish, L. Klein, J. W. Reiner, and M. R. Beasley, Testing the Berry phase model for extraordinary Hall effect in $SrRuO_3$, Phys. Rev. B **70**, 180407(R) (2004).

[31] D. Roy, N. Haham, J. W. Reiner, E. Shimshoni, and L. Klein, Intermixing of ordinary and anomalous Hall effect in $SrRuO_3$, Phys. Rev. B **92**, 235101 (2015).

[32] K. Gupta, B. Mandal, and P. Mahadevan, Strain-induced metal-insulator transition in ultrathin films of $SrRuO_3$, Phys. Rev. B **90**, 125109 (2014).

[33] P. Werner, E. Gull, M. Troyer, and A. J. Millis, Spin Freezing Transition and Non-Fermi-Liquid Self-Energy in a Three-Orbital Model, Phys. Rev. Lett. **101**, 166405 (2008).

[34] S. Roy, C. Autieri, B. Sanyal, and T. Banerjee, Interface control of electronic transport across the magnetic phase transition in $SrRuO_3/SrTiO_3$ heterointerface, Sci. Rep. **5**, 15747 (2015).

[35] M. Ziese, I. Vrejoiu, and D. Hesse, Structural symmetry and magnetocrystalline anisotropy of $SrRuO_3$ films on $SrTiO_3$, Phys. Rev. B **81**, 184418 (2010).

[36] Y. Ohuchi, J. Matsuno, N. Ogawa, Y. Kozuka, M. Uchida, Y. Tokura, and M. Kawasaki, Electric-field control of anomalous and topological Hall effects in oxide bilayer thin films, Nat. Commun. **9**, 213 (2018).

[37] A. Kanbayasi, Magnetocrystalline anisotropy of $SrRuO_3$, J. Phys. Soc. Jpn. **41**, 1879 (1976).

[38] L. Klein, J. S. Dodge, C. H. Ahn, J. W. Reiner, L. Mieville, T. H. Geballe, M. R. Beasley, and A. Kapitulnik, Transport and magnetization in the badly metallic itinerant ferromagnet, J. Phys.: Condens. Matter **8**, 10111 (1996).

[39] See Supplemental Material at http://link.aps.org/supplemental/10.1103/PhysRevResearch.2.032026 for further details on growth and magnetotransport on other films studied, detailed analysis on scaling behavior of the AHE, numerical simulations including DMI contribution and discussions on coexisting magnetic ground states using DFT.

[40] I. Lindfors-Vrejoiu and M. Ziese, Topological Hall effect in antiferromagnetically coupled $SrRuO_3/La_{0.7}Sr_{0.3}MnO_3$ epitaxial heterostructures, Phys. Status Solidi B **254**, 1600556 (2017).

[41] T. Garel and S. Doniach, Phase transitions with spontaneous modulation-the dipolar Ising ferromagnet, Phys. Rev. B **26**, 325 (1982).

[42] X. Yu, M. Mostovoy, Y. Tokunaga, W. Zhang, K. Kimoto, Y. Matsui, Y. Kaneko, N. Nagaosa, and Y. Tokura, Magnetic stripes and skyrmions with helicity reversals, Proc. Natl. Acad. Sci. USA **109**, 8856 (2012).

[43] A. P. Malozemoff and J. C. Slonczewski, *Magnetic Domain Walls in Bubble Materials* (Academic, New York, 1979).

[44] A. Hubert and R. Schäfer, *Magnetic Domains* (Springer, Berlin, 1998).

[45] C. Kooy, Experimental and theoretical study of the domain configuration in thin layers of $BaFe_{12}O_{19}$, Philips Res. Rep. **15**, 7 (1960).

[46] M. Vousden, M. Albert, M. Beg, M.-A. Bisotti, R. Carey, D. Chernyshenko, D. Cortés-Ortuño, W. Wang, O. Hovorka, C. H. Marrows *et al.*, Skyrmions in thin films with easy-plane magnetocrystalline anisotropy, Appl. Phys. Lett. **108**, 132406 (2016).

[47] S. A. Montoya, S. Couture, J. J. Chess, J. C. T. Lee, N. Kent, D. Henze, S. K. Sinha, M.-Y. Im, S. D. Kevan, P. Fischer *et al.*, Tailoring magnetic energies to form dipole skyrmions and skyrmion lattices, Phys. Rev. B **95**, 024415 (2017).